Nano Energy 80 (2021) 105565

Contents lists available at ScienceDirect

Nano Energy

journal homepage: http://www.elsevier.com/locate/nanoen

Full paper

A micro-cavity forming electrode with high thermal stability for semi-transparent colorful organic photovoltaics exceeding 13% power conversion efficiency

Yun-Ming Sung [a], Meng-Zhen Li [b], Dian Luo [c], Yan-De Li [b], Sajal Biring [a], Yu-Ching Huang [d], Chun-Kai Wang [e], Shun-Wei Liu [a,*], Ken-Tseng Wong [e,f,**]

[a] Organic Electronics Research Center and Department of Electronic Engineering, Ming Chi University of Technology, New Taipei City 24301, Taiwan
[b] Department of Electronic Engineering, National Taiwan University of Science and Technology, Taipei 10607, Taiwan
[c] Institute of Lighting and Energy Photonics, National Chiao Tung University, Tainan 71150, Taiwan
[d] Department of Materials Engineering, Ming Chi University of Technology, New Taipei City 24301, Taiwan
[e] Department of Chemistry, National Taiwan University, Taipei 10617, Taiwan
[f] Institute of Atomic and Molecular Science, Academia Sinica, Taipei 10617, Taiwan

ARTICLE INFO

Keywords:
Semi-transparent photovoltaic
Colorful photovoltaic
Micro-cavity
Polymer solar cell
Small molecule solar cell

ABSTRACT

In this study, we demonstrate a novel micro-cavity forming electrode with a sandwiched structure of Ag/HATCN/Ag. This new electrode presents high transmittance in visible wavelengths and reveals the capability of modulating the wavelength of transmitted light by precisely adjusting the thickness of HATCN interlayer. Notably, the Ag/HATCN/Ag electrode possesses excellent thermal stability that leads to an insignificant peak shift of the transmittance spectrum after thermal aging as exposed to air. This new electrode can be applied to both the solution-processed polymer solar cell (PSC) and thermally evaporated small molecule solar cell (SMSC). The implementation of the Ag/HATCN/Ag electrode for the blue, green, and red PSCs with PM6:Y6 as the photoactive blend results in the power conversion efficiency (PCE) over 13%, representing the highest performance for colorful PSCs ever reported. Significantly, the blue PSC shows the highest PCE up to 13.54% with a maximum transmittance of 15.6%. In addition, vacuum-processed red SMSC based on the active layer composed of DTDCPB:C_{70} blend shows a PCE and a maximum transmittance of 7.84% and 26.4%, respectively, while the blue and green SMSCs also exhibit PCE higher than 7%. The high PCE and the good transmittance of both the PSC and SMSC imply that the new micro-cavity forming Ag/HATCN/Ag electrode has promising potential in various practical applications.

1. Introduction

Organic photovoltaics (OPVs) are emerging as one of the promising green and sustainable energy technologies, which have been researched enthusiastically in the last two decades. OPVs offer superior advantages, including low cost, lightweight, flexible, semi-transparent, colorful, and the feasibility for a large area coating. Among various OPVs, solution-processed polymer solar cell (PSC) received the most attractions and research activities mainly due to the flexibility of material design for physical property tuning as well as the potential of roll-to-roll manufacture. Thanks to the invention of the non-fullerene acceptors (NFAs), PSC has a significant breakthrough in recent years. For example, Yuan et al. reported an outstanding NFA, Y6, which combined with a polymer donor PM6 to give PSC with a high power conversion efficiency (PCE) of 15.7% [1]. Subsequently, Pan et al. introduced a small amount of $PC_{71}BM$ to the active layer of PM6:Y6, making a ternary PSC that achieved an improved PCE of ~ 16.7% [2]. This strategy was also adopted by Zhan et al., they reported a PSC based on a ternary blended active layer composing of BTP-M:PM6:Y6 for a broad absorption range that further improved the efficiency record to 17.03% [3]. More recently, PSC with the new active layer composing of a polymer donor D18 and Y6 was demonstrated by Liu et al., giving the device the highest PCE of 18.22% [4]. These excellent results manifest the optimistic future of PSCs to serve as a candidate technology for solar light energy harvesting

* Corresponding author.
** Corresponding author at: Department of Chemistry, National Taiwan University, Taipei 10617, Taiwan.
E-mail addresses: swliu@mail.mcut.edu.tw (S.-W. Liu), kenwong@ntu.edu.tw (K.-T. Wong).

https://doi.org/10.1016/j.nanoen.2020.105565
Received 23 April 2020; Received in revised form 10 September 2020; Accepted 31 October 2020
Available online 4 November 2020

applications. Considering to explore various utilizations of OPVs in our daily life, the OPVs with semi-transparent and/or colorful features may exhibit great potential applications such as building-integrated photovoltaic (BIPV) [5], smart window [6,7], greenhouse [8,9], the decoration of artworks, etc. Typically, PSC is composed of a donor/acceptor blend as the active layer with an optimized thickness of about < 200 nm, which is feasible for creating semi-transparent devices. Generally, semi-transparent and colorful PSC can be achieved by changing the active materials with different absorption spectrum [10], introducing additive [11], or using the electrode with optical design [12]. The absorption spectrum of photovoltaic-active organic material can be reasonably modulated through the custom-design of the chemical structure. However, the unpredictable changes of the active layer by intermixing donor and acceptor could lead to poor device performance due to the morphology related issues. On the other hand, the semi-transparent and/or colorful PSCs can be realized by the optical design of the electrode, regardless of the active materials employed to achieve high PCE [13]. Usually, the optical design strategy of the electrode includes photonic crystals [14–16] and micro-cavity [17,18], which can selectively transmit or reflect the light of desirable wavelength by changing the film thickness of the cavity layers [19]. The micro-cavity is usually formed with the structure configured as semi-transparent metal/dielectric material/semi-transparent metal. For example, Zhong et al. have used PTB7-TH:$PC_{71}BM$ blend to fabricate high performance, semi-transparent, and colorful binary PSC [20]. They deposited Au as the seed layer of Ag and then made high-performance semi-transparent PSC with the efficiency and maximum transmittance of 9% and 21.1%, respectively. Besides, they also fabricated colorful PSC by using the micro-cavity structure of Au/Ag/WO_3/Ag, and the efficiency and maximum transmittance for blue, green, and red PSC are 9.10%, 9.11%, 9.09% and 16.9%, 24.7%, and 24.3%, respectively. More recently, Wang et al. developed an acceptor PTTtID-Cl with a near-infrared absorption profile, which combined with a polymer donor PTB7-Th to fabricate a high performance, semi-transparent, and colorful ternary PSC incorporated 20 nm Ag as the electrode [21], achieving the highest PCE of 10.3%. Colorful PSCs were also fabricated through micro-cavity design, in which Ag (20 nm)/ITO/Ag (20 nm) was implemented as the electrode. The highest PCE and maximum transmittance for blue, green, and red PSC are 8.7%, 8.4%, 9.1% and 26.4%, 16.3%, 11.6%, respectively. These results show promising prospects of semi-transparent and colorful PSCs. However, the stability that is the most crucial factor for the practical application of these colorful and semi-transparent PSCs is rarely discussed in the literature.

Herein, we report a novel micro-cavity forming electrode configured as Ag/HATCN/Ag to fabricate semi-transparent and colorful solar cells. This structure not only offers high transmittance and good thermal stability but also can be used in both solution-processed PSC and thermally evaporated small molecule solar cell (SMSC). The blue, green, and red bare electrodes exhibit high transmittance and insignificant peak shift even after 13 hours of heat treatment at 85 °C as exposed to air. This new electrode was employed to fabricate a high-performance inverted PSC with PM6:Y6 as the active layer of the device structure configured as ITO/ZnO nanoparticles (ZnO NPs)/PEIE/PM6:Y6/MoO_3/electrode. The reference PSC with the electrode of 100 nm Ag shows the PCE of 15.13%, which is comparable to the outstanding efficiency reported by other groups [3,22,23]. Excitingly, the micro-cavity based colorful PSC retains good efficiency of 13.54%, 13.46%, and 13.30% for the blue, green, and red PSC, respectively, representing hitherto the highest PCEs reported for semi-transparent and colorful PSCs based on the best of our knowledge. Interestingly, the color of the semi-transparent PSC could be tuned to red even the active layer is in blue. To our delight, the micro-cavity structure of Ag/HATCN/Ag also works very well in SMSC fabricated by thermal evaporation. The device structure of the SMSC is configured as ITO/MoO_3/DTDCPB:C_{70}/BCP/electrode, in which the active layer DTDCPB:C_{70} has been reported to achieve the highest PCE of OPV by vacuum deposition [24]. The reference SMSC with the electrode of 100 nm Ag exhibits a PCE of 8.42%, while the PCE for blue, green, and red SMSC is 7.69%, 7.66%, 7.69%, respectively. Our results pave a new avenue to realize the fabrication of highly efficient colorful and semi-transparent OPVs.

2. Experimental section

2.1. Materials

PM6 and Y6 were purchased from 1-materials. PEIE, bathocuproine (BCP), C_{70}, MoO_3, and Ag were purchased from Sigma-Aldrich. HATCN was purchased from Shine materials. The DTDCPB was synthesized in our group [25,26] and ZnO NPs was synthesized by the method reported by Wang et al. [27].

2.2. Fabrication of colored electrodes

The electrodes of Ag/HATCN, MoO_3, NPB/Ag were deposited on cleaned glasses by thermal evaporation under 2×10^{-6} torr. The thickness of Ag in all color electrodes is 30 nm. In the case of Ag/HATCN/Ag and Ag/NPB/Ag structure, the thickness of HATCN is 70 nm, 95 nm, and 120 nm for the blue, green, and red color electrode. On the other hand, the thickness of MoO_3 is 50 nm, 85 nm, and 120 nm for the blue, green, and red color electrode with the structure of Ag/MoO_3/Ag.

2.3. Device fabrication

The 15 Ω/□ patterned ITO glasses were cleaned by 1% detergent water (Hellmanex III, Ossila), DI water, and isopropanol in an ultrasonic bath and then dried by flowing nitrogen gas. Then, the ITO glasses were further cleaned by UV-ozone for 20 mins. For the solution-processed PSC, the ZnO NPs solution was spin-coated on cleaned ITO glasses at 3000 rpm for 30 s. Then, 0.4 wt% PEIE was coated on ZnO NPs film at 3000 rpm for 30 s and then annealed at 110 °C for 10 mins to remove the residue solvents. The PM6:Y6 solution (1:1.2, 16 mg/mL in chloroform with 0.5% 1-chloronaphthalene) was spin-coated on previously coated substrates at 4000 rpm for 30 s and then annealed at 110 °C for 10 mins. Then, 7 nm MoO_3 was thermally evaporated on the active layer under 2×10^{-6} torr. After MoO_3 deposition, the PSC was completed by deposition of 100 nm Ag, 30 nm Ag and 30 nm Ag/HATCN/30 nm Ag for the reference, semi-transparent and colorful PSC application. For the thermally evaporated conventional SMSC fabrication process, 15 nm MoO_3 was deposited on cleaned ITO glasses at 0.25 Å/s under 5×10^{-6} torr. The active layer of 80 nm DTDCPB:C_{70} (1:2, 0.3 Å/s for the donor) was co-deposited on MoO_3 film. Then, 3 nm BCP was deposited on the active layer at 0.3 Å/s. Finally, the SMSC was completed by the deposition of the top electrode with the same recipe to the PSC.

2.4. Device characterization

The solar cell performance was measured by AAA class AM 1.5G solar simulator (SS-X100R, Enlitech) with a 0.04 cm^2 shadow mask. The light intensity was calibrated by silicon standard reference. The external quantum efficiency (EQE) measurement was conducted by solar cell spectral response measurement (QE-R3011, Enlitech). The UV–vis spectrum measurement was measured by a UV–visible spectrophotometer (V-770, JASCO). All the optical simulation was conducted by SETFOS simulation software (Fluxim). The AFM measurements were measured by using a desktop AFM instrument (Innova, BRUKER).

3. Results and discussion

3.1. Properties of Ag/HATCN/Ag

A novel micro-cavity forming system configured as Ag/HATCN/Ag was proposed in this study to control the wavelength of the transmitted

lights by tuning the thickness of the sandwiched HATCN layer. The thin Ag film serves as a semi-transparent electrode as well as takes part in forming the optical cavity for the OPV device simultaneously. The optical cavity formed by the two Ag thin films enhances the multiple reflections of the incident lights with the wavelengths having integral multiples of the cavity length (optical path), which could be controlled by the thickness of the inserted HATCN layer. Thus, a specific wavelength favors constructive interference inside the optical cavity and leads to the enhanced intensity of the corresponding wavelength. In general, the transmittance and bandwidth of the transmitted light are strongly dependent on the thickness of the ultrathin Ag layer [28,29]. The transmittances of the semi-transparent electrode with various Ag thicknesses (10, 30, and 50 nm) were simulated using SETFOS simulation software (Fluxim). As shown in Fig. S1a (Supplementary Information, SI), the 10 nm Ag thin film shows a higher transmittance, i.e., T% $>$ 60% at 550 nm, compared to those with thicker Ag films. However, a thin Ag film cannot perform the desired function of transmitting the specific spectrum through the electrode due to a weaker micro-cavity

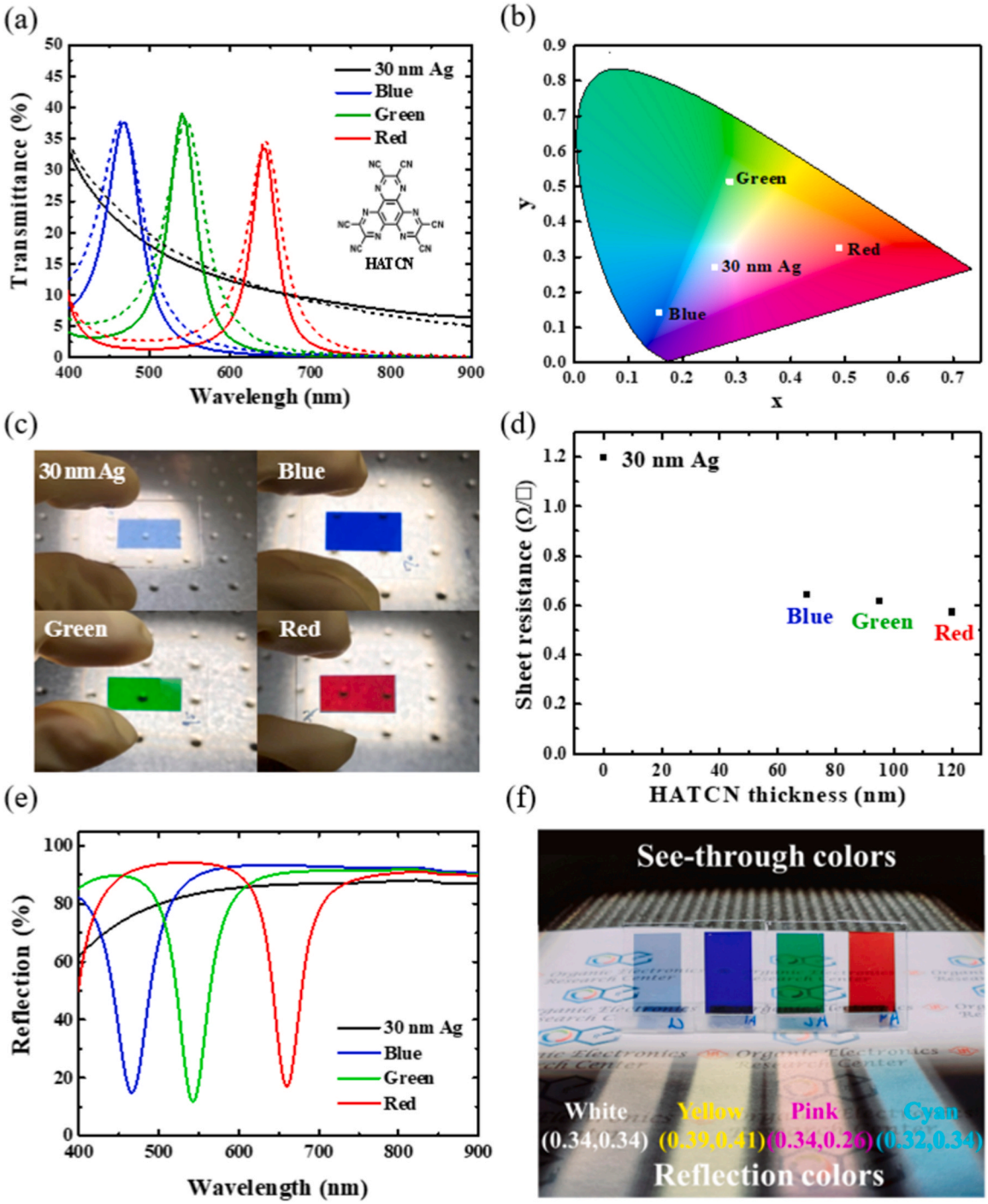

Fig. 1. (a) Experimental (solid line) and simulated (dashed line) transmittance spectrum with the molecular structure of HATCN inserted in the inset. (b) the CIE 1931 coordinates of blue, green, and red electrodes. (c) The see-through colors of real-devices under 1 sun illuminance. (d) The sheet resistance and (e) the reflection spectra of colorful Ag/HATCN/Ag micro-cavity electrodes. (f) The decoration of the micro-cavity electrode with vivid see-through/reflection color applications under the light intensity of ~ 0.5 sun.

effect in the active layer. On the other hand, the transmittance spectra of the micro-cavity electrodes, i.e., Ag/HATCN/Ag, with various Ag thicknesses (10, 30, and 50 nm) and HATCN thicknesses (70, 95, and 120 nm) were simulated as shown in Fig. S1b–d. The transmission profile of the colorful electrodes with the Ag thickness of 10 nm shows a wide full width at half maximum (FWHM) of > 300 nm, i.e., the colorful electrode offers low color purity. Whereas, the transmission spectra of the colorful electrodes with Ag thickness of 30 nm reveal narrow peaks with FWHM < 60 nm at specific wavelength depending on the thickness of HATCN, resulting in the improvement of the color purity. In addition, the micro-cavity electrode with 30 nm Ag shows the transmittance of > 35% to each color, i.e., blue, green, and red under the indoor light or sunlight. Note that the thickness of the central HATCN layer selected for the blue, green, and red colored OPVs is 70 nm, 95 nm, and 120 nm, respectively. However, when the thickness of Ag increases to 50 nm, the FWHM of the transmission spectrum reduces to < 40 nm which can be ascribed to the strong cavity effect resulting in lowering transmittance to < 10%. Therefore, the proposed Ag/HATCN/Ag electrode with 30 nm Ag layer is the best choice as the semi-transparent electrode that was applied in this study considering the trade-off between the transmittance and conductivity (as discussed later).

Fig. 1 shows the transmittance data, the CIE 1931 coordinates, the sheet resistance, reflection data, as well as the photographs of the Ag/HATCN/Ag electrodes under the illumination of simulated sunlight. The experimental and simulated transmittance data of the semi-transparent and colorful electrodes agree well, as depicted in Fig. 1a. The small mismatch could be ascribed to the film inhomogeneity or the variation in the refractive index and extinction coefficient of materials. The average transmittance of a 30 nm Ag film is 13.22% from 400 to 900 nm, whereas the maximum transmittance of blue, green, and red electrodes is 34.42%, 39.04%, and 33.56% at 465 nm, 540 nm, and 640 nm, respectively. The color purity of these electrodes is demonstrated by the color coordinates in the CIE 1931 diagram, as presented in Fig. 1b. Obviously, the CIE coordinates of a 30 nm Ag film (0.259, 0.272) is competently different from other colorful electrodes (Ag/HATCN (x nm)/Ag), such as blue (CIE: 0.157, 0.142; x = 70), green (CIE: 0.287, 0.514; x = 95), and red (CIE: 0.489, 0.325; x = 120). The visualization of the colorful electrodes under the simulated sunlight (100 mW/cm^2; 1 sun) is illustrated in Fig. 1c, revealing the attractive colorful features. Moreover, the conductivity of the colorful Ag/HATCN/Ag electrode is better as compared to that of a 30 nm Ag film, as shown in Fig. 1d. The measured sheet resistance of a 30 nm Ag electrode and the colorful electrode (Ag/HATCN/Ag) is 1.2 Ω/□ and 0.6 Ω/□, respectively. Interestingly, the colorful electrodes possess better conductivity regardless of the thickness of the HATCN layer. The effect of the sheet resistance was also investigated in the electrical performance of the OPVs, which will be discussed later. It is worthy to note that the micro-cavity electrodes may show the transmission color during daytime but the reflection color during nighttime because the top or bottom side has a specific reflection spectrum. As shown in Fig. 1e, the reflectance spectrum of the Ag/HATCN/Ag electrode shows a particular resonance peak compared to the transmittance spectrum (Fig. 1a), which means the light can transmit through the micro-cavity electrode in the device to display the "see-through color" and reflect the complementary color for generating the "reflection color". Regarding such optical phenomena, the decoration applications of our micro-cavity electrodes with vivid see-through/reflection colors can be feasibly manifested as indicated in Fig. 1f. As a result, this new electrode can present both of the transmission and reflection colors in visible wavelengths by precisely adjusting the thickness of the HATCN interlayer.

More importantly, the possibility of making a large area colorful electrode is pivotal for BIPV or smart window applications. Note that the new micro-cavity forming colorful electrodes demonstrate good uniformity and transmittance even with the active size of 5 cm × 5 cm, as shown in Fig. S2a. In addition, a large-area and multi-colored fuzzy electrode can be also achieved by tilted fabrication process (Fig. S2b). Furthermore, the colorful electrode can also work nicely under low light intensity. For example, as the green electrode was illuminated under an indoor light (TL84 light source) at the intensity of 1588 lux, 562 lux, and 191 lux, that still can transmit the selected wavelength, suggesting the feasibility for indoor applications (Fig. S3).

3.2. Thermal stability of Ag/HATCN/Ag

The thermal stability of the colorful electrode comprising multiple layers is an important issue for practical light energy harvesting applications. The thermal inter-diffusion of the adjacent layers could decrease the effective thickness of the optical cavity and then lead to a blue shift of the transmittance spectrum. Considering this issue, the thermal stability of the transmittance spectra and surface morphology of the electrode configured as Ag/HATCN/Ag, Ag/MoO_3/Ag, and Ag/NPB/Ag were examined under 85 °C for 13 hours as exposed to air following the ISOS-D2 protocol. The obtained transmittance spectra of blue, green, and red electrodes are shown in Fig. 2a–c, respectively. As indicated in Fig. 2, the Ag/HATCN/Ag shows a negligible change in maximum transmittance, in which only the red electrode exhibits a slightly blue shift of 5 nm. The atomic force microscopy (AFM) images, as shown in Fig. S4, reveals that the Ag/HATCN/Ag has high thermal stability. The surface roughness of pristine Ag/HATCN/Ag for blue, green, and red electrode is 2.51 nm, 3.14 nm, and 3.23 nm, respectively. After the thermal aging, the surface roughness slightly changes to 2.69 nm, 3.13 nm, and 3.27 nm for blue, green, and red electrode, respectively. According to the research published by Frank et al. [30], the HATCN grown on Ag (111) has a strong CN–Ag bond, and its crystallinity retains highly stable even at the temperature up to 400 K. Hence, the high thermal stability of Ag/HATCN/Ag can be attributed to the high crystallinity of HATCN and the strong binding between HATCN and Ag. For the limited blue shift of the red-colored Ag/HATCN/Ag electrode, we speculate that such shift is caused by the diffusion of Ag to the defects of HATCN film as the increased thickness of HATCN film or the small aggregation of Ag after thermal aging as observed in AFM images. On the other hand, the green and red electrodes with the structure of Ag/MoO_3/Ag show a much evident blue shift of 16 nm and 27 nm, respectively. The surface roughness (Fig. S5) of the pristine blue, green, and red Ag/MoO_3/Ag electrode is 7.48 nm, 5.46 nm, and 4.68 nm, respectively. After the thermal aging, the surface roughness increases to 8.18 nm, 5.97 nm, and 5.17 nm for blue, green, and red Ag/MoO_3/Ag electrode, respectively. This phenomenon can be rationalized by taking into account of the unstable interfacial surface between MoO_3 and Ag according to the study with AFM and Rutherford backscattering spectrometry for probing the change upon the heat treatment at 85 °C reported by Greenbank et al. [31]. Therefore, the clear blue shift of green and red Ag/MoO_3/Ag can be attributed to the serious thermal diffusion at the MoO_3/Ag interface. Similarly, the blue, green, and red electrodes configured with the structure of Ag/NPB/Ag show a 12 nm blue shift after thermal aging. The pristine surface morphology, as shown in Fig. S6, shows a smooth surface with the surface roughness of 2.41 nm, 1.71 nm, and 1.02 nm for blue, green, and red electrodes. After thermal aging, the surface roughness for blue, green, and red electrodes dramatically increase to 5.41 nm, 5.84 nm, and 6.70 nm, respectively. The reason for the blue shift and significant change in morphology can be mainly attributed to the low glass transition temperature of NPB (about 98 °C) [32], which could lead to NPB re-distribution and serious diffusion at the NPB/Ag interface. Based on these studies, the new Ag/HATCN/Ag electrodes have been verified with good thermal stability, together with the high transmittances in various wavelength ranges, rendering them excellent candidates for practical semi-transparent and colorful OPV applications.

3.3. Solution-processed semi-transparent and colorful PSC

The Ag/HATCN/Ag with optimized transmittance and color purity

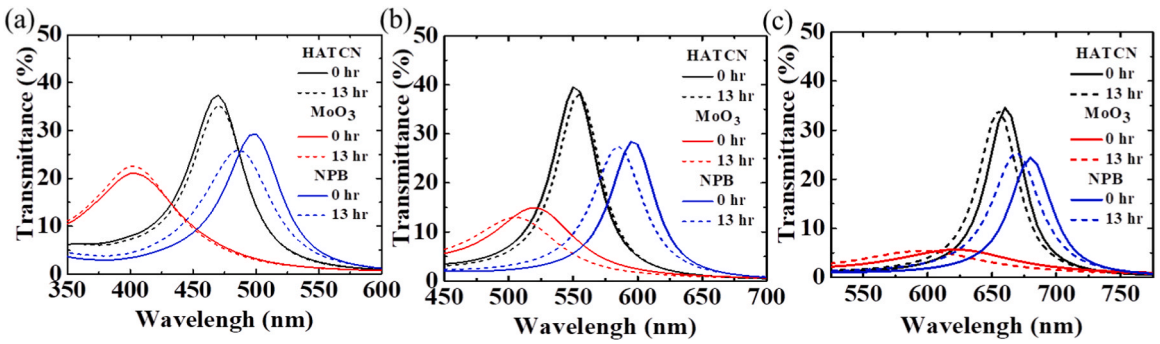

Fig. 2. The transmittance spectrum of the colorful electrode with the structure of Ag/HATCN/Ag, Ag/MoO_3/Ag, and Ag/NPB/Ag for (a) Blue, (b) Green, and (c) Red electrodes with and without thermal heating treatment at 85 °C for 13 h as exposed to air.

was then applied to fabricate solution-processed PSC, where PM6 and Y6 were used as the polymer donor and non-fullerene acceptor, respectively. The chemical structures of the organic materials, the device structure of the PSC, and the energy diagram of the constituent materials are displayed in Fig. 3.

Inverted PSCs with the device structure of ITO/ZnO NPs/PEIE/PM6:Y6/MoO_3/electrode were fabricated, where 100 nm Ag, 30 nm Ag, and Ag/HATCN/Ag electrode have opted for the reference, semi-transparent, and colorful PSC, respectively. The structure of Ag/HATCN/Ag selected for the designated colorful PSC was adopted based on the fabrication of the colorful electrode mentioned earlier. PEIE was introduced as a surface modifier to decrease the defect and improve the contact between ZnO NPs and the active layer [33–35]. The current–voltage, EQE, simulated and experimental transmittance, and device photos of the obtained PSCs are shown in Fig. 4. The device characteristics, maximum transmittance, and color coordinates are summarized in Table 1. The reference PSC with a 100 nm Ag as electrode showed the PCE of 15.13% with short-circuit current (J_{sc}), open-circuit voltage (V_{oc}), and fill factor (FF) of 26.41 mA/cm^2, 0.82 V, and 70.09%, respectively, which are comparable to the data reported by other groups [3,15,16,22]. The PCE of the semi-transparent PSC with a 30 nm Ag electrode plummeted to 12.69% with the J_{sc}, V_{oc}, and FF of 24.09 mA/cm^2, 0.80 V, and 65.73% (See Fig. 4a), respectively. The decrease in J_{sc} can be reasonably attributed to the loss of light absorption, which is caused by the average device transmittance of 3.92% in the wavelength range from 400 to 900 nm. Hence, the EQE of the semi-transparent PSC is lower than that of the reference PSC as observed in Fig. 4b. Besides, a 30 nm Ag film has higher sheet resistance compared to a 100 nm Ag film, which is another viable reason for the low V_{oc} and FF [36]. On the other hand, the blue PSC shows the highest PCE of 13.54% with J_{sc}, V_{oc}, and FF of 24.60 mA/cm^2, 0.81 V, and 67.79%, respectively. The CIE 1931 color coordinates, as shown in Fig. S7a, for blue, green, and red PSC are (0.144, 0.118), (0.295, 0.532), and (0.453, 0.266), respectively. Interestingly, all the colorful PSCs show similar performances, which are higher than that of the semi-transparent PSC. This phenomenon can be plausibly explained by the EQE and transmittance data presented in Fig. 4b and c, respectively. As indicated in Fig. 4b, the EQE data exhibit dips at 470 nm, 550 nm, and 655 nm for blue, green, and red PSC, respectively. These results are well consistent with the transmittance spectrum, which means the dips can be attributed to the loss of the absorbed light. However, it still showed about 16 nm difference between the valley of the EQE spectrum and the peak

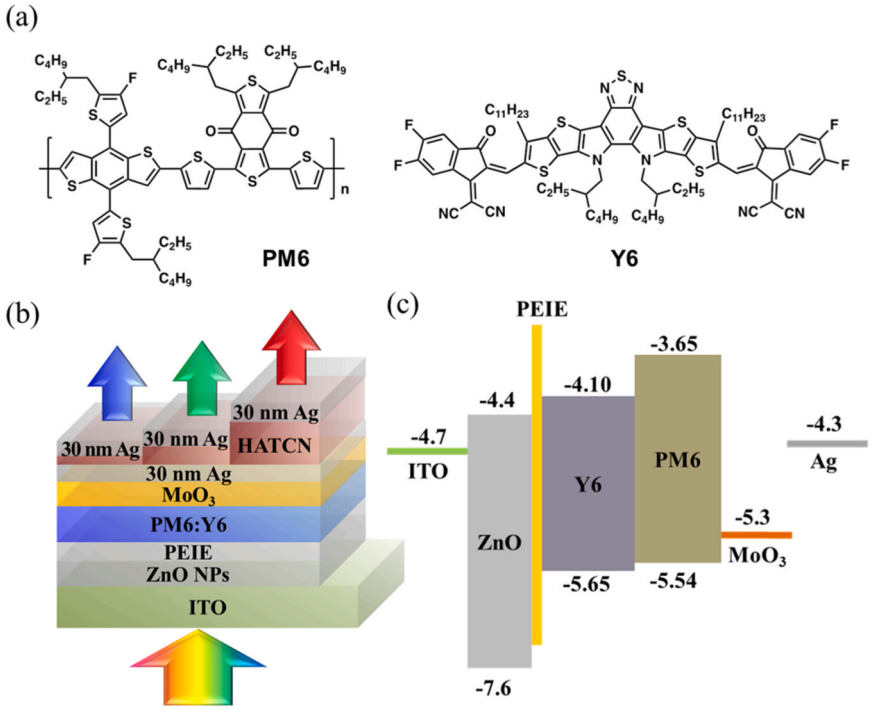

Fig. 3. (a) The chemical structures of PM6 and Y6, (b) solution-processed inverted PSC structure, and schematic of colorful PSC, and (c) energy level of PSC.

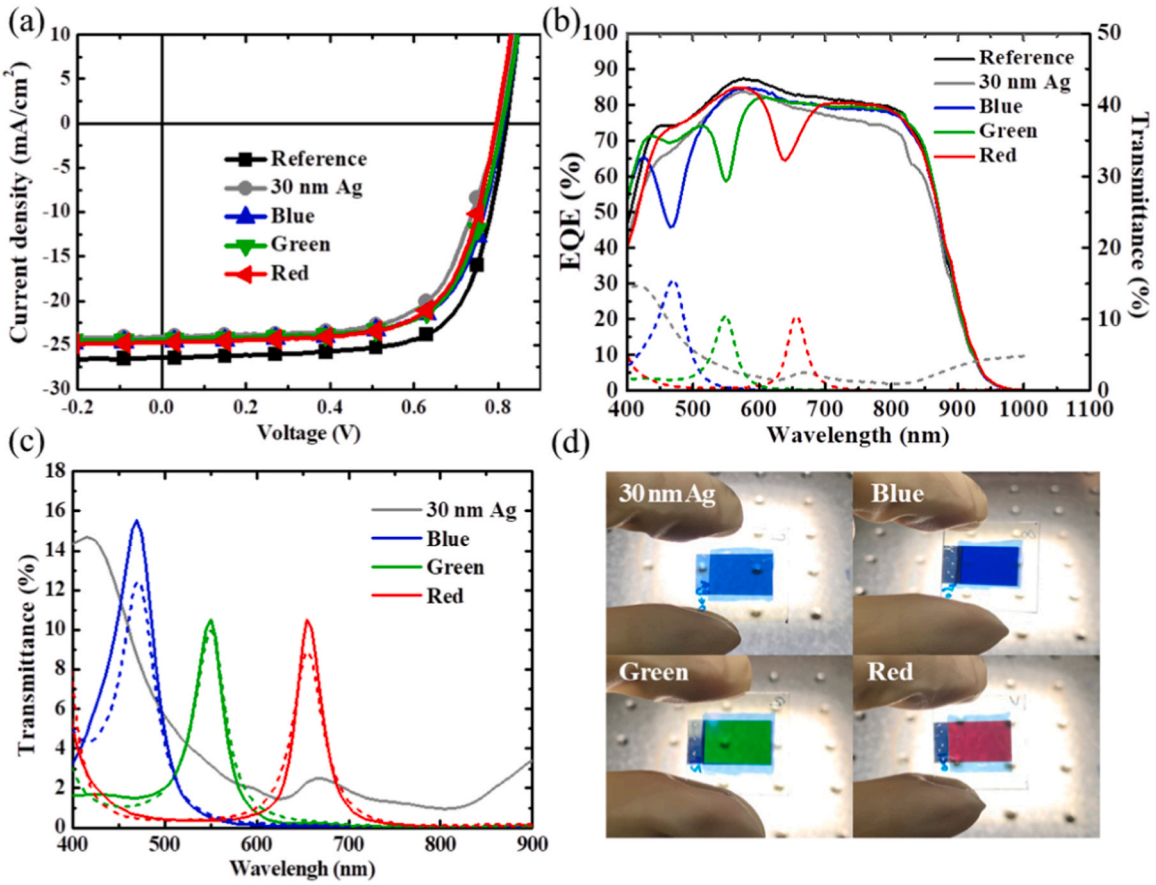

Fig. 4. (a) The current density-voltage data, (b) experimental EQE (solid line) and transmittance (dashed line) spectrum, (c) experimental (solid line) and simulated (dashed line) transmittance spectrum, and (d) the photographs of the semi-transparent and colorful PSCs.

Table 1
The summary of the electrical characteristic, current density calculated from EQE (J_{EQE}), maximum transmittance, and CIE 1931 color coordinates of the PSCs.[a]

Device	J_{SC} (mA cm^{-2})	V_{OC} (V)	FF (%)	PCE (%)	J_{EQE} (mA cm^{-2})	T_{max} (nm, %)	CIE 1931 (x, y)
100 nm Ag	26.17 ± 0.24	0.82 ± 0.00	69.10 ± 0.13	14.92 ± 0.14	25.52	–	–
30 nm Ag	24.49 ± 0.39	0.80 ± 0.01	64.09 ± 1.28	12.63 ± 0.05	23.88	–	–
Blue	24.64 ± 0.20	0.81 ± 0.00	65.99 ± 1.24	13.28 ± 0.30	24.36	(470, 15.6)	(0.144, 0.118)
Green	24.29 ± 0.23	0.81 ± 0.00	65.79 ± 1.57	12.90 ± 0.39	24.23	(550, 10.4)	(0.295, 0.532)
Red	24.75 ± 0.44	0.80 ± 0.00	65.07 ± 1.63	12.94 ± 0.30	24.52	(655, 10.5)	(0.453, 0.266)

[a] The values of the standard deviation for each parameter are calculated based on the measurement of eight devices.

of the transmittance curve of the red-color device as the similar mismatch result was found in the previous work [17]. Such phenomena could be probably ascribed to the absorption profile and crystallinity of the active layer that consequentially contribute to the unique distribution of optical fields, leading to the peak mismatch between the EQE and transmittance curve. In addition, the incident light from the glass side and the reflected light from the top electrode would form a standing wave in the active layer. That could also possibly lead to the mismatch between EQE and transmittance at a specific wavelength.

Besides, the J_{sc} of all the colorful PSCs are higher than that of the semi-transparent PSC. As mentioned in the previous discussion, the semi-transparent PSC exhibits a full band transmittance with an average transmittance of 3.92%. However, the colorful PSC only transmits the light of the selected wavelength, which means the Ag/HATCN/Ag electrode is capable of showing good color purity even after the deposition of the active layer, which can absorb more light except for the selected wavelength compared to the semi-transparent PSC. Moreover, all the colorful PSCs show similar performances with various thicknesses of HATCN, implying no damage occurred on the active layer during the thermal evaporation process. Fig. 4c depicts the measured and the simulated transmittance data of Ag/HATCN/Ag electrodes used in OPV, considering the materials under the Ag/HATCN/Ag are air for bare electrode and active layer for PSC, respectively. Clearly, the transmittance peaks of colorful PSCs show insignificant shifts compared to the bare Ag/HATCN/Ag electrodes. The limited peak shifts can be plausibly attributed to the difference in refractive index and extinction coefficient caused by the different materials under the Ag/HATCN/Ag electrode. Fig. 4d shows the photographs of semi-transparent and colorful PSCs. Interestingly, the colorful PSC exhibits pure red even the active layer of PM6:Y6 with the blue color, which means our Ag/HATCN/Ag structure can be applied to various kinds of materials regardless of the original color of the active materials. Then, the measurements of the reflection spectrum of PSC were carried out from the top (micro-cavity side) and bottom (glass side) as shown in Fig. S8. In consequence, the Ag/HATCN/Ag electrode shows a strong resonance effect and tunable spectrum under the light illuminated from the top side. In contrast, such phenomena were not observed in the case that the light illuminated from the bottom side because the active absorption

layer could curtail the light in the device. To ensure the accurate value was obtained in this work, the independent EQE, T, and R of each sample were measured carefully to avoid the uncertain errors. Accordingly, the summed values (Fig. S9) of EQE + T + R are < 1 for both of the device with 30 nm Ag and reference device (100 nm), corroborating no overestimation issue in this work.

Recently, perovskite-based solar cells received high attention, mainly due to the amazing high PCEs. Up to now, a PCE of 25.2% for a single-cell perovskite-based photovoltaic was achieved and reported by NREL [37]. However, the variation in the active layer thickness of perovskite solar cells decreases its transmittance and increases the hysteresis effect [38]. Hence, retaining both high performance and transmittance is crucial to semi-transparent and colorful perovskite solar cells. Recently, Tong et al. have developed a high-efficiency semi-transparent perovskite solar cell with a PCE of 18.2% [39]. In case of the colorful perovskite solar cells, the highest PCE is 18.9% and 11.18% for the reflected and transmitted mode, respectively [40,41]. Our new micro-cavity embedded colorful and semi-transparent OPV exhibiting the respective PCE of 13.54%, 13.46%, and 13.30% for the blue, green, and red device is the record-high efficiency even compared to the decent perovskite-based solar cells for the transmitted mode.

3.4. Thermal evaporated semi-transparent and colorful SMSC

To test the generality of the micro-cavity effect of Ag/HATCN/Ag electrode, the Ag/HATCN/Ag structure was exploited to SMSCs fabricated with thermal evaporation. The device structure of the SMSCs, chemical structures, and energy diagram of the constituent materials are presented in Fig. 5. The device structure of the SMSC is configured as ITO/MoO_3/DTDCPB:C_{70}/BCP/electrode. This configuration is similar to the structure reported by Forrest group for the champion devices both in single and tandem cells [42,43]. The electrodes were adopted similar to our PSC devices, i.e., 100 nm Ag, 30 nm Ag, and Ag/HATCN/Ag for reference, semi-transparent, and colorful SMSCs, respectively.

Fig. 6 depicts the current-voltage characteristics, EQE data, experimental and simulated transmittance data, and the photographs of the colorful SMSCs. The details of the device performance, maximum transmittance, and CIE 1931 color coordinates of the SMSCs are summarized in Table 2. The PCE of the reference SMSC is 8.35% with J_{sc}, V_{oc}, and FF of 13.62 mA/cm^2, 0.88 V, and 69.7%, respectively. On the contrary, the semi-transparent SMSC exhibits inferior device performance with PCE, J_{sc}, V_{oc}, and FF of 7.38% 12.07 mA/cm^2, 0.88 V, and 69.5%, respectively. The average transmittance of the semi-transparent SMSC in the visible wavelengths is 9.8%, which is higher than that of the solution-processed PSC. Such a high transmission value can be attributed to that the relatively lower thickness of the active layer, DTDCPB:C_{70}, which is only 80 nm in SMSC compared to that 120 nm of PM6:Y6 in PSC (See Fig. S9). The lower J_{sc} of semi-transparent SMSC compared to that of the reference device stems from the lower EQE values in the wavelength range spanning from 400 to 800 nm. As far as the colorful SMSCs are concerned, the red device shows the highest PCE of 7.84% with J_{sc}, V_{oc}, and FF of 12.52 mA/cm^2, 0.89 V and 69.85%, respectively. Besides, the CIE 1931 color coordinates (Fig. S7b) of blue, green, and red SMSCs are (0.158, 0.193), (0.278, 0.518), and (0.499, 0.301), respectively. In addition, the EQE data exhibit dips at 486 nm, 556 nm, and 681 nm, which are well consistent with the transmittance data. Similar to the solution-processed PSCs, all the colorful SMSCs show higher EQEs than that of the semi-transparent SMSC, which suggests that the colorful SMSC transmits the selected wavelength effectively and benefits from the lower absorption loss. Besides, the higher EQE of the red SMSC can be attributed to the low absorption of DTDCPB:C_{70} at 681 nm, leading to the highest transmittance. Furthermore, all the blue, green, and red SMSCs show similar device performance. These results of transmission (See Fig. 6c) or reflection (see Fig. S10) are in consistent with solution-processed PSCs and justify the applicability of micro-cavity forming structure of Ag/HATCN/Ag to various optical systems.

4. Conclusion

A novel micro-cavity-forming electrode configured as Ag/HATCN/Ag was developed to control the wavelength of transmitted light by changing HATCN thickness. Such a structure shows not only high transmittance but also stable thermal stability. The optimized Ag/HATCN/Ag electrodes were applied to fabricate both colorful solution-

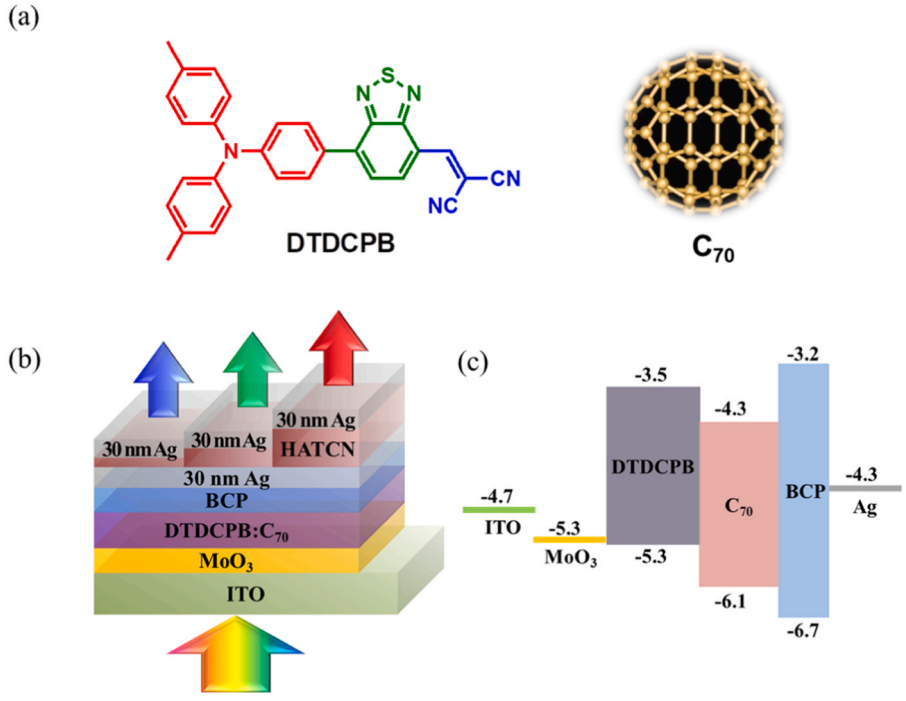

Fig. 5. (a) Chemical structures of DTDCPB and C_{70}, (b) schematic device structure of thermally evaporated SMSC and colorful SMSC, and (c) energy level diagram of materials used in SMSC.

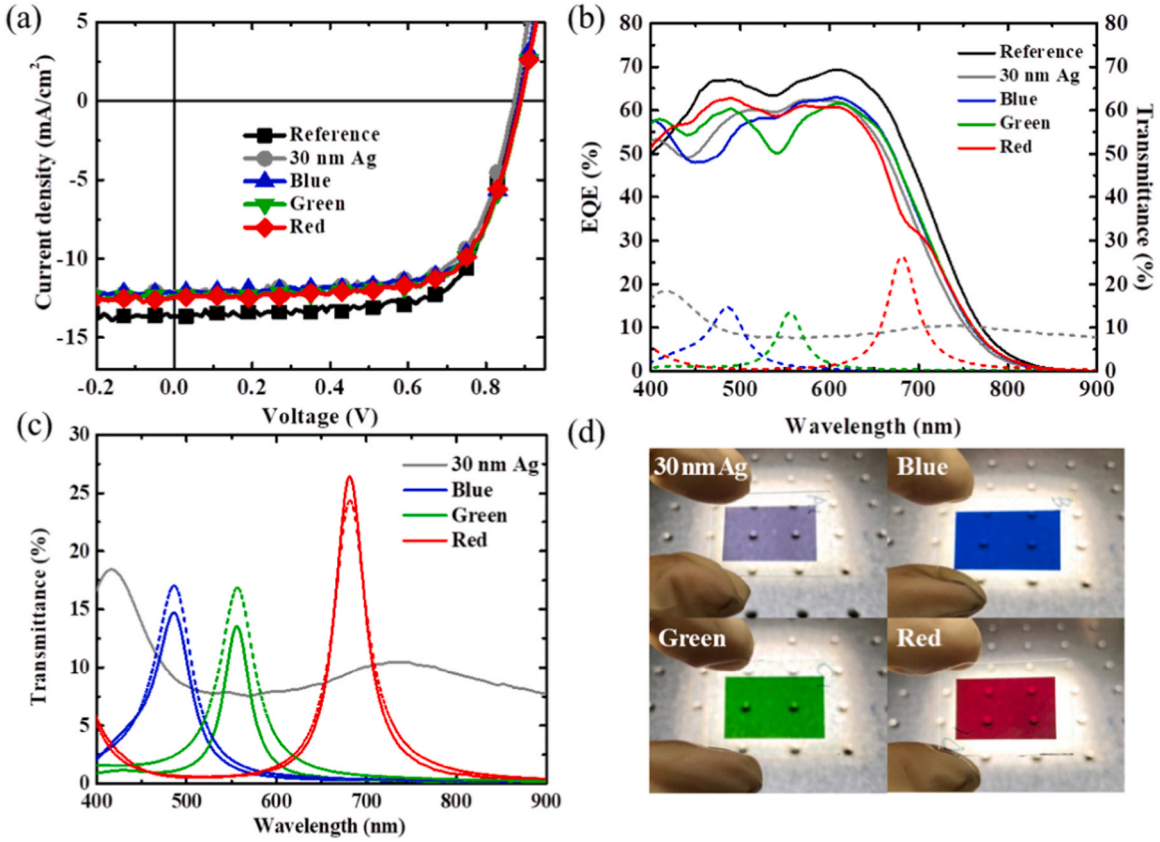

Fig. 6. (a) The current density-voltage data, (b) experimental EQE (solid line) and transmittance (dashed line) data, (c) experimental (solid line) and simulated (dashed line) transmittance spectrum and (d) photographs of semi-transparent, and thermally evaporated colorful SMSCs.

Table 2
Summary of the electrical characteristics, current density calculated from EQE (J_{EQE}), maximum transmittance, and CIE 1931 color coordinates of SMSCs.[a]

Device	J_{SC} (mA cm^{-2})	V_{OC} (V)	FF (%)	PCE (%)	J_{EQE} (mA cm^{-2})	T_{max} (nm, %)	CIE 1931 (x, y)
100 nm Ag	13.58 ± 0.13	0.87 ± 0.00	69.87 ± 0.79	8.28 ± 0.07	13.53	–	–
30 nm Ag	12.11 ± 0.13	0.86 ± 0.01	69.34 ± 0.53	7.25 ± 0.10	11.99	–	–
Blue	11.92 ± 0.23	0.90 ± 0.01	69.52 ± 0.65	7.42 ± 0.18	12.15	(486, 14.7)	(0.158,0.193)
Green	12.04 ± 0.20	0.90 ± 0.01	69.80 ± 0.60	7.52 ± 0.09	12.16	(556, 13.5)	(0.278,0.518)
Red	11.93 ± 0.23	0.89 ± 0.00	69.01 ± 0.96	7.36 ± 0.13	12.19	(681, 26.4)	(0.499,0.301)

[a] The values of the standard deviation for each parameter are calculated based on the measurement of eight devices.

processed PSC and thermally evaporated SMSC. In the case of solution-processed inverted PSC incorporating PM6:Y6 blend as active layer, the blue PSC showed the highest PCE of 13.54% with the color coordinates and maximum transmittance of (0.144, 0.118) and 15.6%, respectively. On the other hand, the red thermally evaporated SMSC based on the active blend of DTDCPB:C_{70} showed the highest PCE and high maximum transmittance of 7.84% and 26.4%, respectively with the color coordinates of (0.499, 0.301). All the colorful devices show similar device performance regardless of the device color in either PSC or SMSC, which suggests that the fabrication of the novel micro-cavity structure of Ag/HATCN/Ag does not damage the active layer during the deposition process. Hence, we believe this micro-cavity forming Ag/HATCN/Ag electrode can be a good candidate for good performance colorful and semi-transparent OPVs for future BIPV applications.

CRediT authorship contribution statement

Yun-Ming Sung: Conceptualization, Polymer solar cell fabrication and analysis, Topography analysis, Writing manuscript. **Meng-Zhen Li:** Small molecular solar cell fabrication and analysis. **Dian Luo:** Simulation. **Yan-De Li:** Small molecular solar cell fabrication and analysis. **Sajal Biring:** Reviewing and editing manuscript. **Yu-Ching Huang:** Reviewing and editing manuscript. **Chun-Kai Wang:** Materials synthesis. **Shun-Wei Liu:** Conceptualization, Electrode design, Reviewing and editing manuscript. **Ken-Tseng Wong:** Conceptualization, Reviewing and editing manuscript.

Declaration of Competing Interest

The authors declare that they have no known competing financial interests or personal relationships that could have appeared to influence the work reported in this paper.

Acknowledgments

This work was supported by the Ministry of Science and Technology (grant numbers MOST 107-2113-M-002-019-MY3, 107-2218-E-131-007-MY3, 107-2221-E-131-029-MY2, 107-2119-M-131-001, 108-2221-E-131-027-MY2, 108-2221-E-011-151, 109-2223-E-131-001-MY3). Also, the corresponding author (S.-W. Liu) is grateful to Mr. H.-H. Wu, Syskey Technology Corporation (Taiwan), for his assistance in designing the fabrication system.

Appendix A. Supporting information

Supplementary data associated with this article can be found in the online version at doi:10.1016/j.nanoen.2020.105565.

References

[1] J. Yuan, Y. Zhang, L. Zhou, G. Zhang, H.-L. Yip, T.-K. Lau, X. Lu, C. Zhu, H. Peng, P. A. Johnson, M. Leclerc, Y. Cao, J. Ulanski, Y. Li, Y. Zou, Single-junction organic solar cell with over 15% efficiency using fused-ring acceptor with electron-deficient core, Joule 3 (2019) 1140–1151, https://doi.org/10.1016/j.joule.2019.01.004.

[2] M.-A. Pan, T.-K. Lau, Y. Tang, Y.-C. Wu, T. Liu, K. Li, M.-C. Chen, X. Lu, W. Ma, C. Zhan, 16.7%-efficiency ternary blended organic photovoltaic cells with PCBM as the acceptor additive to increase the open-circuit voltage and phase purity, J. Mater. Chem. A 7 (2019) 20713–20722, https://doi.org/10.1039/C9TA06929A.

[3] L. Zhan, S. Li, T.-K. Lau, Y. Cui, X. Lu, M. Shi, C.-Z. Li, H. Li, J. Hou, H. Chen, Over 17% efficiency ternary organic solar cells enabled by two non-fullerene acceptors working in an alloy-like model, Energy Environ. Sci. 13 (2020) 635–645, https://doi.org/10.1039/C9EE03710A.

[4] Q. Liu, Y. Jiang, K. Jin, J. Qin, J. Xu, W. Li, J. Xiong, J. Liu, Z. Xiao, K. Sun, S. Yang, X. Zhang, L. Ding, 18% Efficiency organic solar cells, Sci. Bull. 65 (2020) 272–275, https://doi.org/10.1016/j.scib.2020.01.001.

[5] D. Chemisana, A. Moreno, M. Polo, C. Aranda, A. Riverola, E. Ortega, Chr. Lamnatou, A. Domènech, G. Blanco, A. Cot, Performance and stability of semitransparent OPVs for building integration: a benchmarking analysis, Renew. Energy 137 (2019) 177–188, https://doi.org/10.1016/j.renene.2018.03.073.

[6] F. Guo, S. Chen, Z. Chen, H. Luo, Y. Gao, T. Przybilla, E. Spiecker, A. Osvet, K. Forberich, C.J. Brabec, Printed smart photovoltaic window integrated with an energy-saving thermochromic layer, Adv. Opt. Mater. 3 (2015) 1524–1529, https://doi.org/10.1002/adom.201500314.

[7] M. Yao, T. Li, Y. Long, P. Shen, G. Wang, C. Li, J. Liu, W. Guo, Y. Wang, L. Shen, X. Zhan, Color and transparency-switchable semitransparent polymer solar cells towards smart windows, Sci. Bull. 65 (2020) 217–224, https://doi.org/10.1016/j.scib.2019.11.002.

[8] C.J.M. Emmott, J.A. Röhr, M. Campoy-Quiles, T. Kirchartz, A. Urbina, N.J. Ekins-Daukes, J. Nelson, Organic photovoltaic greenhouses: a unique application for semi-transparent PV? Energy Environ. Sci. 8 (2015) 1317–1328, https://doi.org/10.1039/C4EE03132F.

[9] H. Shi, R. Xia, G. Zhang, H.-L. Yip, Y. Cao, Spectral engineering of semitransparent polymer solar cells for greenhouse applications, Adv. Energy Mater. 9 (2019), 1803438, https://doi.org/10.1002/aenm.201803438.

[10] Y. Cui, C. Yang, H. Yao, J. Zhu, Y. Wang, G. Jia, F. Gao, J. Hou, Efficient semitransparent organic solar cells with tunable color enabled by an ultralow-bandgap nonfullerene acceptor, Adv. Mater. 29 (2017), 1703080, https://doi.org/10.1002/adma.201703080.

[11] J. Kong, M.M. Beromi, M. Mariano, T.H. Goh, F. Antonio, N. Hazari, A.D. Taylor, Colorful polymer solar cells employing an energy transfer dye molecule, Nano Energy 38 (2017) 36–42, https://doi.org/10.1016/j.nanoen.2017.05.032.

[12] K.-T. Lee, J.Y. Lee, S. Seo, L.J. Guo, Colored ultrathin hybrid photovoltaics with high quantum efficiency, Light Sci. Appl. 3 (2014), e215, https://doi.org/10.1038/lsa.2014.96.

[13] S. Shafian, J. Son, Y. Kim, J.K. Hyun, K. Kim, Active-material-independent color-tunable semitransparent organic solar cells, ACS Appl. Mater. Interfaces 11 (2019) 18887–18895, https://doi.org/10.1021/acsami.9b03254.

[14] Y. Zhang, Z. Peng, C. Cai, Z. Liu, Y. Lin, W. Zheng, J. Yang, L. Hou, Y. Cao, Colorful semitransparent polymer solar cells employing a bottom periodic one-dimensional photonic crystal and a top conductive PEDOT:PSS layer, J. Mater. Chem. A 4 (2016) 11821–11828, https://doi.org/10.1039/C6TA05249E.

[15] J. Liu, M. Yao, L. Shen, Third generation photovoltaic cells based on photonic crystals, J. Mater. Chem. C 7 (2019) 3121–3145, https://doi.org/10.1039/C8TCs05461D.

[16] P. Shen, M. Yao, J. Liu, Y. Long, W. Guo, L. Shen, Colored semitransparent polymer solar cells with a power conversion efficiency of 9.36% achieved by controlling the optical Tamm state, J. Mater. Chem. A 7 (2019) 4102–4109, https://doi.org/10.1039/C9TA00227H.

[17] J.-H. Lu, Y.-H. Lin, B.-H. Jiang, C.-H. Yeh, J.-C. Kao, C.-P. Chen, Microcavity structure provides high-performance (>8.1%) semitransparent and colorful organic photovoltaics, Adv. Funct. Mater. 28 (2018), 1703398, https://doi.org/10.1002/adfm.201703398.

[18] Y. Li, C. Ji, Y. Qu, X. Huang, S. Hou, C.-Z. Li, L.-S. Liao, L.J. Guo, S.R. Forrest, Enhanced light utilization in semitransparent organic photovoltaics using an optical outcoupling architecture, Adv. Mater. 31 (2019), 1903173, https://doi.org/10.1002/adma.201903173.

[19] Y.-H. Chen, C.-W. Chen, Z.-Y. Huang, W.-C. Lin, L.-Y. Lin, F. Lin, K.-T. Wong, H.-W. Lin, Microcavity-embedded, colour-tuneable, transparent organic solar cells, Adv. Mater. 26 (2014) 1129–1134, https://doi.org/10.1002/adma.201304658.

[20] J. Zhong, Z. Xiao, W. Liang, Y. Wu, Q. Ye, H. Xu, H. Deng, L. Shen, X. Feng, Y. Long, Highly efficient and high peak transmittance colorful semitransparent organic solar cells with hybrid-electrode-mirror microcavity structure, ACS Appl. Mater. Interfaces 11 (2019) 47992–48001, https://doi.org/10.1021/acsami.9b19174.

[21] C.-K. Wang, B.-H. Jiang, J.-H. Lu, M.-T. Cheng, R.-J. Jeng, Y.-W. Lu, C.-P. Chen, K.-T. Wong, A near-infrared absorption small molecule acceptor for high-performance semitransparent and colorful binary and ternary organic photovoltaics, ChemSusChem 13 (2020) 903–913, https://doi.org/10.1002/cssc.201903087.

[22] K. Jiang, Q. Wei, J.Y.L. Lai, Z. Peng, H.K. Kim, J. Yuan, L. Ye, H. Ade, Y. Zou, H. Yan, Alkyl chain tuning of small molecule acceptors for efficient organic solar cells, Joule 3 (2019) 3020–3033, https://doi.org/10.1016/j.joule.2019.09.010.

[23] B. Liu, Y. Wang, P. Chen, X. Zhang, H. Sun, Y. Tang, Q. Liao, J. Huang, H. Wang, H. Meng, X. Guo, Boosting efficiency and stability of organic solar cells using ultralow-cost BiOCl nanoplates as hole transporting layers, ACS Appl. Mater. Interfaces 11 (2019) 33505–33514, https://doi.org/10.1016/j.joule.2019.09.010.

[24] S. Biring, Y.-M. Sung, T.P. Nguyen, Y.-Z. Li, C.-C. Lee, A.H.Y. Chan, B. Pal, S. Sen, S.-W. Liu, K.-T. Wong, Reconciling the value of Schottky barriers in small molecular organic photovoltaics from J-V and C-V measurements at low temperatures towards the estimation of open circuit voltage at 0 K, Org. Electron. 73 (2019) 166–171, https://doi.org/10.1016/j.orgel.2019.06.014.

[25] Y.-H. Chen, L.-Y. Lin, C.-W. Lu, F. Lin, Z.-Y. Huang, H.-W. Lin, P.-H. Wang, Y.-H. Liu, K.-T. Wong, J. Wen, D.J. Miller, S.B. Darling, Vacuum-deposited small-molecule organic solar cells with high power conversion efficiencies by judicious molecular design and device optimization, J. Am. Chem. Soc. 134 (2012) 13616–13623, https://doi.org/10.1021/ja301872s.

[26] L.-Y. Lin, Y.-H. Chen, Z.-Y. Huang, H.-W. Lin, S.-H. Chou, F. Lin, C.-W. Chen, Y.-H. Liu, K.-T. Wong, A low-energy-gap organic dye for high-performance small-molecule organic solar cells, J. Am. Chem. Soc. 133 (2011) 15822–15825, https://doi.org/10.1021/ja205126t.

[27] H. Wang, C. Xie, W. Zhang, S. Cai, Z. Yang, Y. Gui, Comparison of dye degradation efficiency using ZnO powders with various size scales, J. Hazard. Mater. 141 (2007) 645–652, https://doi.org/10.1016/j.jhazmat.2006.07.021.

[28] K.-T. Lee, J.Y. Lee, S. Seo, L.J. Guo, Microcavity-integrated colored semitransparent hybrid photovoltaics with improved efficiency and color purity, IEEE J. Photovolt. 5 (2015) 1654–1658, https://doi.org/10.1109/JPHOTOV.2015.2478063.

[29] K.-T. Lee, H.W. Baac, D.H. Park, J.G. Ok, H.J. Park, Enhanced optical properties of colored semitransparent ultrathin hybrid solar cells employing Fabry–Pérot Etalon with a dielectric overlay, IEEE Photonics J. 10 (2018), 8400510, https://doi.org/10.1109/JPHOT.2018.2876397.

[30] P. Frank, T. Djuric, M. Koini, I. Salzmann, R. Rieger, K. Müllen, R. Resel, N. Koch, A. Winkler, Layer growth, thermal stability, and desorption behavior of hexaaza-triphenylene-hexacarbonitrile on Ag(111), J. Phys. Chem. C 114 (2010) 6650–6657, https://doi.org/10.1021/jp100704v.

[31] W. Greenbank, L. Hirsch, G. Wantz, S. Chambon, Interfacial thermal degradation in inverted organic solar cells, Appl. Phys. Lett. 107 (2015), 263301, https://doi.org/10.1063/1.4938554.

[32] Q.-X. Tong, S.-L. Lai, M.-Y. Chan, K.-H. Lai, J.-X. Tang, H.-L. Kwong, C.-S. Lee, S.-T. Lee, High T_g triphenylamine-based starburst hole-transporting material for organic light-emitting devices, Chem. Mater. 19 (2007) 5851–5855, https://doi.org/10.1021/cm0712624.

[33] B.A.E. Courtright, S.A. Jenekhe, Polyethylenimine interfacial layers in inverted organic photovoltaic devices: effects of ethoxylation and molecular weight on efficiency and temporal stability, ACS Appl. Mater. Interfaces 7 (2015) 26167–26175, https://doi.org/10.1021/acsami.5b08147.

[34] L.K. Jagadamma, M. Al-Senani, A. El-Labban, I. Gereige, G.O.N. Ndjawa, J.C. D. Faria, T. Kim, K. Zhao, F. Cruciani, D.H. Anjum, M.A. McLachlan, P. M. Beaujuge, A. Amassian, Polymer solar cells with efficiency >10% enabled via a facile solution-processed Al-doped ZnO electron transporting layer, Adv. Energy Mater. 5 (2015), 1500204, https://doi.org/10.1002/aenm.201500204.

[35] R.M. Hewlett, M.A. McLachlan, Surface structure modification of ZnO and the impact on electronic properties, Adv. Mater. 28 (2016) 3893–3921, https://doi.org/10.1002/adma.201503404.

[36] J.-W. Kang, S.-P. Lee, D.-G. Kim, S. Lee, G.-H. Lee, J.-K. Kim, S.-Y. Park, J.H. Kim, H.-K. Kim, Y.-S. Jeong, Reduction of series resistance in organic photovoltaic using low sheet resistance of ITO electrode, Electrochem. Solid-State Lett. 12 (2009) H64–H66, https://doi.org/10.1149/1.3055339.

[37] National Renewable Energy Laboratory (NREL), Best Research-Cell Efficiency Chart, ⟨https://www.nrel.gov/pv/cell-efficiency.html⟩.

[38] A.-N. Cho, I.-H. Jang, J.-Y. Seo, N.-G. Park, Dependence of hysteresis on the perovskite film thickness: inverse behavior between TiO_2 and PCBM in a normal planar structure, J. Mater. Chem. A 6 (2018) 18206–18215, https://doi.org/10.1039/C8TA04919J.

[39] J. Tong, Z. Song, D.H. Kim, X. Chen, C. Chen, A.F. Palmstrom, P.F. Ndione, M. O. Reese, S.P. Dunfield, O.G. Reid, J. Liu, F. Zhang, S.P. Harvey, Z. Li, S. T. Christensen, G. Teeter, D. Zhao, M.M. Al-Jassim, M.F.A.M. van Hest, M.C. Beard, S.E. Shaheen, J.J. Berry, Y. Yan, K. Zhu, Carrier lifetimes of >1 μs in Sn-Pb perovskites enable efficient all-perovskite tandem solar cells, Science 364 (2019) 475–479, https://doi.org/10.1126/science.aav7911.

[40] G.Y. Yoo, R. Azmi, C. Kim, W. Kim, B.K. Min, S.-Y. Jang, Y.R. Do, Stable and colorful perovskite solar cells using a nonperiodic SiO_2/TiO_2 multi-nanolayer filter, ACS Nano 13 (2019) 10129–10139, https://doi.org/10.1021/acsnano.9b03098.

[41] K.-T. Lee, J.-Y. Jang, N.Y. Ha, S. Lee, H.J. Park, High-performance colorful semitransparent perovskite solar cells with phase-compensated microcavities, Nano Res. 11 (2018) 2553–2561, https://doi.org/10.1007/s12274-017-1880-0.

[42] X. Che, Y. Li, Y. Qu, S.R. Forrest, High fabrication yield organic tandem photovoltaics combining vacuum- and solution-processed subcells with 15% efficiency, Nat. Energy 3 (2018) 422–427, https://doi.org/10.1038/s41560-018-0134-z.

[43] Y. Li, J.-D. Lin, X. Liu, Y. Qu, F.-P. Wu, F. Liu, Z.-Q. Jiang, S.R. Forrest, Near-infrared ternary tandem solar cells, Adv. Mater. 30 (2018), 1804416, https://doi.org/10.1002/adma.201804416.

Dr. Yun-Ming Sung recieved his M.S. and Ph.D. degree in Physics from National Taiwan University (NTU) in 2011 and 2015. He joined the Institute of Nuclear Energy Research for the development of large area coating process in 2015–2018. He is currently Postdoctoral fellow in the Organic Electronics Research Center and Department of Electronic Engineering, Ming Chi University of Technology. His research focus on the high performance polymer and small molecular solar cells, devices stability and the analysis of carrier transport. He also focus on the development of large-area manufacture of the polymer solar cells using sheet-to-sheet and roll-to-roll techniques.

Meng-Zhen Li got her B.S. degree from the Department of Electronic Engineering, Ming Chi University of Technology (MCUT) in 2018, and M.S. degree from the Department of Electronic and Computer Engineering, National Taiwan University of Science and Technology (NTUST) in 2020. Her research topics include small molecule and polymer organic solar cells, focusing on device performance optimization and structural design.

Dian Luo got his M.S. degree from Department of Electrical Engineering, Yuan Ze University (YZU) in 2018. He is currently working toward the Ph.D. degree in Institute of Lighting and Energy Photonics, National Chiao Tung University (NCTU). His research areas are the development of organic light emitting diodes (OLEDs) with different emitting system including phosphorescence, thermally activated delayed fluorescence (TADF) and exciplex. He has co-authored 11 refereed journal papers. Now he is working on the OLEDs with exciplex host and the organic solar cells with functional electrode.

Yan-De Li got his B.S. degree from the Department of Electronic Engineering, Ming Chi University of Technology (MCUT) in 2017, and M.S. degree from the Department of Electronic and Computer Engineering, National Taiwan University of Science and Technology (NTUST) in 2019. He focuses on device structure design and optical simulation of organic light emitting diodes (OLEDs) and organic photovoltaics (OPVs).

Dr. Sajal Biring is currently (starting from 2016) an assistant professor in the Department of Electronic Engineering, Ming Chi University of Technology (MCUT), as well as the head of the research division in the organic electronics research center in MCUT. His current research interests lie in developing artificially intelligent sensing technologies based on organic optoelectronic devices i.e., photovoltaic driven image devices, indoor photovoltaics, near-infrared exciplex organic light-emitting diodes, and ultra-thin/flexible electronics. Until now, Dr. Biring has published over 100 international journal papers and dozens of patents. Dr. Biring has prolonged work experience in semiconductor industries in Taiwan and China.

Dr. Yu-Ching Huang recieved his B.S. degree in Chemical Engineering from National Taiwan University (NTU) in 2003, and recieved his M.S. and Ph.D. degree in Materials Science and Engineering from NTU in 2005 and 2010, respectively. He joined the Institute of Nuclear Energy Research (INER) as a deputy engineer from 2010 to 2018. Now he is an assistant professor in the Department of Materials Engineering at Ming Chi University of Technology (MCUT). His research focuses on the large-area manufacture of the organic photovoltaics, and the nanostructure analysis of organic electronics using the grazing-incident small-angle and wide-angle X-ray scattering.

Dr. Chun-Kai Wang received his Ph.D. degree from the Department of Chemistry at National Taiwan University in 2019. His research mainly focuses on the molecular design and synthesis of novel ladder-type π-conjugated materials for optoelectronic applications such as organic field-effect transistors and organic photovoltaics.

Dr. Shun-Wei Liu is currently a distinguished professor in the Department of Electronic Engineering, Ming Chi University of Technology (MCUT), as well as the director of the Organic Electronics Research Center in MCUT. His current research interests are in the area of understanding the fundamental physics of organic materials and their relevance in novel optoelectronic devices, i.e., indoor small molecule/perovskite PVs, OLED medical/beauty patches, and transparent displays. Until now, Prof. Liu has published over 130 international journal papers. The details of the laboratory's core facility can be found in the website (http://organicelectronics.mcut.edu.tw/bin/home.php?Lang=en).

Dr. Ken-Tseng Wong, Ph.D. degree, National Taiwan University in 1993, postdoctoral researches at University of Illinois at Urbana-Champaign in 1995–1996 and Université Louis Pasteur, Strasbourg in 1996–1998. He joined the Department of Chemistry at National Taiwan University as an assistant professor in 1998, promoted to an associate professor in 2002 and professor in 2006. His research mainly focuses on the molecular design and organic synthesis of novel π-conjugated materials for optoelectronic applications such as OLED, electrogenerated chemiluminescence (ECL), solid-state light-emitting electrochemical cells (LEC), and photovoltaic devices. Ken has published more than 300 SCI papers in these fields.